Temporally and frequency multiplexed single photon source using quantum feedback control for scalable photonic quantum technologies

Mikkel Heuck,[1,2,*] Mihir Pant,[1] and Dirk Englund[1,†]

[1] *Department of Electrical Engineering and Computer Science, Massachusetts Institute of Technology, 77 Massachusetts Avenue, Cambridge, Massachusetts 02139, USA*

[2] *DTU Fotonik, Department of Photonics Engineering, Technical University of Denmark, Building 343, 2800 Kgs. Lyngby, Denmark*

(Dated: August 30, 2017)

Current proposals for scalable photonic quantum technologies require on-demand sources of indistinguishable single photons with very high efficiency (having unheralded loss below 1%). Even with recent progress in the field there is still a significant gap between the requirements and state of the art performance. Here, we propose an on-chip source of multiplexed, heralded photons. Using quantum feedback control on a photon storage cavity with an optimized driving protocol, we estimate an on-demand efficiency of 99% and unheralded loss of order 1%, assuming high efficiency detectors and intrinsic cavity quality factors of order 10^8. We further explain how temporal- and frequency-multiplexing can be used in parallel to significantly reduce device requirements if single photon frequency conversion is possible with efficiency in the same range of 99%.

I. INTRODUCTION

Achieving sources of on-demand pure single photon states has been a long-standing goal of quantum information science [1]. Recent years have seen considerable progress in the performance of 'deterministic sources' based on two-level quantum emitters [2–4]. Additionally, the efficiency of sources based on probabilistic processes, such as parametric down-conversion and spontaneous four-wave mixing (sFWM), has been improved by multiplexing either spatial [5], temporal [6, 7], or frequency [8] degrees of freedom of photons. Despite this progress, a large gap remains between state of the art demonstrations and the requirements of proposed quantum information processing technologies, including photonic quantum repeaters [9], precision sensors [10], and photonic quantum computing [11, 12]. We believe this calls for investigations into novel device concepts that are necessary to bridge this gap.

In this work, we investigate the feasibility of single photon sources that meet the requirements of scalable photonic quantum technologies: near-unity purity single photons produced in a reproducable chip-integrated photonic circuit. Our proposal uses temporal multiplexing of parametrically produced signal-idler photon pairs and we explain how additional multiplexing of the frequency degree of freedom may lead to significantly improved performance.

We consider a control protocol based on Bayesian inference with both idler and signal photon detection to optimize the signal-photon state. This approach shows the trade-off between heralding the generation of a single photon state and its purity. Our study reveals that, for near-term realistic device parameters, highly efficient ($\sim 99\%$) sources of single photons could be possible in scalable nanophotonic platforms. As illustrated in Fig. 1, our proposed device consists of a high-Q microring resonator (Q of 10-100M) consisting of a material, such as silicon, with a $\chi^{(3)}$ nonlinearity for photon pair generation by sFWM. This storage ring is coupled to photon number resolving detectors (PNRDs) through Mach-Zehnder inferometer (MZI) filters [13]. The filters enable decoupling of certain frequencies from the waveguide by controlling the path-imbalance of the MZI relative to the length of the ring (see inset in Fig. 1). Idler photons and the pump field couple out of the storage ring within a single time bin, whereas the signal can be stored for up to M bins. The signal- and output filters contain tunable

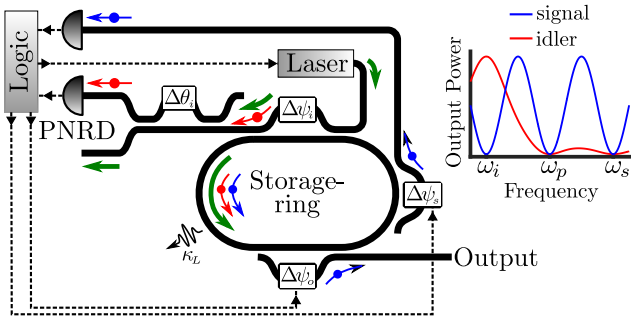

FIG. 1. Storage- and release design. Solid lines are optical waveguides, while dashed lines represent electrical control signals. PNRD: photon number resolving detector. The inset illustrates the power spectrum coupled out of the signal filter in its closed configuration and the spectrum arriving at the idler detector.

phases, $\Delta\psi_s(t)$ and $\Delta\psi_o(t)$, allowing them to dynamically couple out signal photons to a detector or output waveguide, respectively. Each emission cycle is divided into M time bins in which we either: (i) Pump to generate a photon pair; (ii) release excess signal photons by tuning the phase of the signal filter; (iii) evacuate all

* mheu@fotonik.dtu.dk
† englund@mit.edu

photons from the system through the signal filter; or (*iv*) store the signal state if detection events suggest a single photon is present. The driving protocol prescribes which action is taken in a given time bin depending on the information available from detection events. We optimize the protocol to maximize the probability of a single signal photon occupying the storage ring at the emission time, t_M. Signal photons are emitted by tuning the output filter to its open state. Tailoring the temporal shape of $\Delta\psi_o(t)$ allows shaping the output photon wavepacket. Note that signal-idler pairs are generated in single spectral modes of the storage ring in contrast to bulk-optics approaches to store-and-release multiplexing [6, 7, 14]. For a detailed analysis of the architecture, we refer to section I of the supplementary material (SM. I).

This letter is organized as follows: Section II presents the model and probability analysis for evaluating the performance of our proposed architecture and Section III discusses the driving protocol. Section IV presents simulation results and Section V concludes with a discussion of the feasibility of experimental demonstrations.

II. MODEL

The number of time bins available for multiplexing depends on the intrinsic decay rate of the storage ring, κ_L, and the speed of the feedback controls. The mth time bin is defined by the time interval $[t_{m-1},\ t_m]$ and all bins are assumed to be of equal length, $\tau_{\rm bin} = t_m - t_{m-1}$. The feedback controls are the pump power, $|S_{\rm pump}(t)|^2$, and signal filter phase, $\Delta\psi_s(t)$. The processing time of the logic unit, τ_D, determines the necessary lag between the time of deciding the action in bin m+1, t_{m^*}, and its onset, $t_m = t_{m^*} + \tau_D$. If $N_I(t_m)$ and $N_S(t_m)$ denote the number of idler and signal detections up until t_m, the detection number is defined as

$$d^{(m)} \equiv N_I(t_m) - N_S(t_m). \tag{1}$$

We infer the state of the storage ring at t_m based on the value of the detection number at the decision time, t_{m^*}. For instance, $d^{(m^*)} = 1$ suggests that one signal photon occupies the cavity at t_m, which we denote as $n^{(m)} = 1$. If $d^{(m^*)} \geq 0$, our estimation is $n^{(m)}_{\rm est} = d^{(m^*)}$. Since idler photons may not be detected, the detection number can be negative and in this case we always pump the cavity and our estimation is therefore $n^{(m)}_{\rm est} = d^{(m^*)} - d^{(m-1)}$.

The state estimation fidelity is the probability that our estimate of the state is correct, and is given by

$$P(n^{(m)}_{\rm est}|\boldsymbol{d}^{(m^*)}) = \frac{P(n^{(m)}_{\rm est}, \boldsymbol{d}^{(m^*)})}{P(\boldsymbol{d}^{(m^*)})}. \tag{2}$$

The detection sequence $\boldsymbol{d}^{(m^*)} \equiv \{d^{(0)}, d^{(1)}, \ldots, d^{(m-1)}, d^{(m^*)}\}$ contains information from all previous bins. Fig. 2 illustrates two examples of detection sequences leading to successful state preparation. We consider the photon generation successful only if the heralding efficiency (probability of having a single photon in the cavity conditioned on the given detection sequence) and the second-order correlation obey the threshold conditions

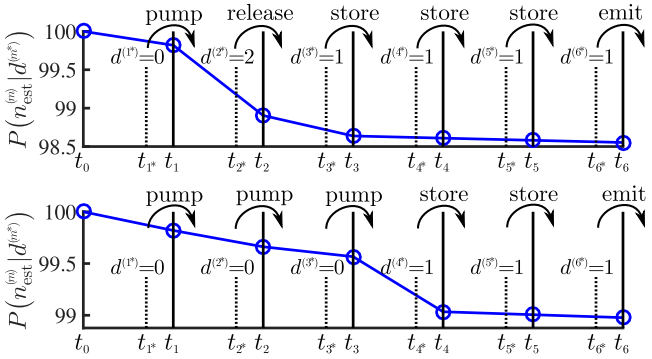

FIG. 2. State estimation fidelity as a function of time for two detection sequences and $M = 6$. Arrows indicate the actions prescribed by the driving protocol (see Section III). Parameters are the same as in Fig. 4.

$$P(n^{(M)}=1|\boldsymbol{d}^{(M^*)}) \geq F_{\rm th} \quad \textit{and} \quad g^{(2)}(\boldsymbol{d}^{(M^*)}) \leq g^{(2)}_{\rm th}, \tag{3}$$

where $g^{(2)}(\boldsymbol{d}^{(M^*)})$ is defined by [15]

$$g^{(2)}(\boldsymbol{d}^{(M^*)}) = \frac{\sum_{n^{(M)}} n^{(M)}(n^{(M)}-1)P(n^{(M)}|\boldsymbol{d}^{(M^*)})}{\left[\sum_{n^{(M)}} n^{(M)}P(n^{(M)}|\boldsymbol{d}^{(M^*)})\right]^2}. \tag{4}$$

The success probability is

$$\mathcal{P}(M) = \sum_{\boldsymbol{d}^{(M^*)}} P(n^{(M)}=1, \boldsymbol{d}^{(M^*)}), \tag{5}$$

where the summation runs over all detection sequences fulfilling Eq. (3). In the top panel of Fig. 2, a detection of two idler photons in bin 2 leads to release of signal photons in bin 3. The detection of one signal photon in bin 3 suggests that the desired state is achieved and it is stored until the end of the emission cycle. In the lower panel, the detection of one idler photon in bin 4 leads to the same conclusion.

The system in Fig. 1 can be modeled by considering three modes of the storage ring where the control-phase of the signal filter, $\Delta\psi_s(t)$, is represented by a time-dependent coupling rate, $\kappa_s(t)$, for the signal mode as discussed in SM. I. Photon pair generation is modeled using the Hamiltonian

$$H_{sys} = \Delta_i \hat{a}_i^\dagger \hat{a}_i + \Delta_s \hat{a}_s^\dagger \hat{a}_s + \mathcal{X}\left(\hat{a}_i^\dagger \hat{a}_s^\dagger + \hat{a}_i \hat{a}_s\right), \tag{6}$$

where $\hat{a}_s$ and $\hat{a}_i$ are annihilation operators of the signal and idler modes, respectively. We use normalized units ($\hbar = 1$) and a classical pump rate described by $\mathcal{X}$, which is proportional to the nonlinear coefficient, $\chi^{(3)}$, and the energy of the pump cavity mode. Δ_s and Δ_i are

detunings between the pump frequency and the signal and idler modes, respectively. We used Monte Carlo simulations [16] to evaluate the probability distribution $P(n^{(m)}, \boldsymbol{d}^{(m^*)})$; see SM. II for details. The assumptions are: 1) Detector dark counts are negligible. 2) The idler mode of the cavity is in the vacuum state at the beginning of each bin. 3) If $d^{(m^*)} \leq 0$, then $n^{(m)} \leq 2$, which is a good approximation for the large detection efficiency used in our simulations. 4) The signal coupling rate, $\kappa_s(t)$, can be varied without increasing the loss rate, κ_L, which is equal for all three modes.

Since the storage cavity has many modes separated by a free spectral range, signal and idler pairs are generated in spectral modes symmetrically distributed about the degenerate pump mode. By heralding on multiple idler modes, we can thus multiplex photon generation in the frequency domain in addition to the time domain. This requires frequency conversion of signal photons to the target wavelength [8, 17]. The total success probability from using N_F frequency modes is $\mathcal{P}_{\rm tot} = 1-(1-\mathcal{P})^{N_F}$, assuming perfect conversion efficiency and no reduction in temporal multiplexing efficiency of each frequency channel. As detailed in SM. IA, Bragg-scattering FWM should enable frequency conversion of the different signal photons to a target frequency with near-unity efficiency.

III. DRIVING PROTOCOL

The driving protocol relates information from photon detections to control actions. Fig. 3 depicts which actions are taken in bin $m+1$ depending on the updated probability distribution in bin m, $P(n^{(m)}|\boldsymbol{d}^{(m^*)})$. In some

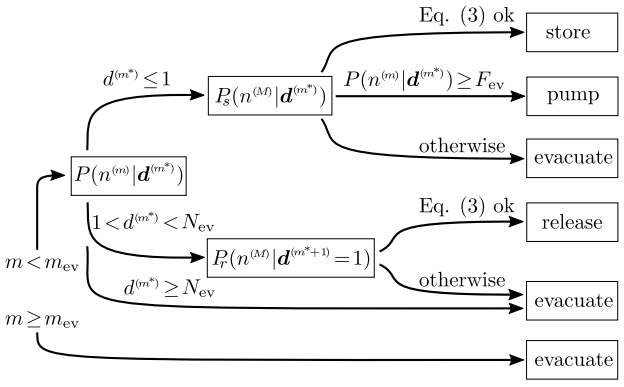

FIG. 3. Diagram illustrating the driving protocol.

parameter regimes, it turns out to be advantageous to evacuate the cavity after a certain number of bins, $m_{\rm ev}$, irrespective of the state estimation fidelity. If $m < m_{\rm ev}$, the protocol depends on $\boldsymbol{d}^{(m^*)}$ in the following way: For $d^{(m^*)} \leq 1$, we evaluate the distribution at the emission time in case the state is stored until then, $P_s(n^{(M)}|\boldsymbol{d}^{(m^*)})$. If Eq. (3) is fulfilled, the state is stored. If not, the next bin is pumped if the fidelity of our current state estimation is larger than the control parameter $F_{\rm ev}$ and otherwise evacuated. For $1 < d^{(m^*)} < N_{\rm ev}$, we calculate the distribution $P_r(n^{(M)}|\boldsymbol{d}^{(m^*+1)}=1)$ corresponding to a release in the next bin followed by storage until the emission time. Again, if the threshold conditions are met by evaluating Eq. (3), we release in the following bin and evacuate otherwise. Note that $N_{\rm ev} = 2$ eliminates release from the four actions described in Section I. SM. III contains more details about the driving protocol.

To optimize the protocol, we start by assuming there is only a single time bin available and iteratively increase M while keeping track of the success probability. When evacuating in bin m, the optimum strategy for the remaining $M-m$ bins is known from a previous iteration. The contribution to the overall success probability is $P(\boldsymbol{d}^{(m^*-1)})\mathcal{P}(M-m)$, where $\boldsymbol{d}^{(m^*-1)}$ is the detection sequence leading us to evacuate in bin m. The iteration continues until Eq. (3) can not be met for larger M. An upper bound on M is found by considering that $F_{\rm th}$ must be larger than the probability of loosing a signal photon within M bins, $\exp[-2\kappa_L M \tau_{\rm bin}]$.

We chose the shape of the pump pulses to be Gaussian, $|S_{\rm pump}(t)|^2 \propto \exp[-(t-t_p)^2/\tau_p^2]$, with $\tau_p = 1$ps. By neglecting self-induced nonlinear effects, the energy in the cavity follows from coupled mode theory [18]

$$\mathcal{X}(t) \propto U_{\rm cav} = \Big| \int_{-\infty}^{t} e^{-\kappa_p (t-t')} S_{\rm pump}(t') dt' \Big|^2. \quad (7)$$

Similarly, the signal filter is controlled by a Gaussian function and has a response time, $1/\kappa_{\psi_s} = 3$ps, such that

$$\kappa_s(t) \propto \int_{t_{m-1}}^{t} e^{-\kappa_{\psi_s}(t-t')} e^{-(t'-t_r)^2/\tau_r^2} dt'. \quad (8)$$

The times t_p and t_r are adjusted such that $\mathcal{X}(t_m - 1)$ and $\kappa_s(t_m - 1)$ are at least a thousand times smaller than their maxima. With fixed temporal profiles of $\mathcal{X}(t)$ and $\kappa_s(t)$, the feedback controls are given by scalars $p^{(m)}$ and $p_c^{(m)}$. $p^{(m)}$ is the probability of creating at least one photon pair in bin m, and $p_c^{(m)}$ is the probability that a photon remains in the cavity during the release process (see SM. IIA and IIB). A fixed pump sequence, $\boldsymbol{p}^{(M)} \equiv \{p^{(1)}, p^{(2)}, \ldots, p^{(M-1)}, p^{(M)}\}$, is used for all detection sequences $\boldsymbol{d}^{(M)}$ unless an evacuation occurs in bin $m < M$. All the control parameters $N_{\rm ev}$, $F_{\rm ev}$, $m_{\rm ev}$, and $\boldsymbol{p}^{(M)}$ are optimized for each M to maximize the success probability. Additionally, $p_c^{(m)}$ is optimized for each bin and $\tau_{\rm bin}$ is optimized for the entire emission cycle. SM. III provides details of the optimization procedure.

IV. SIMULATION RESULTS

The system performance is evaluated by fixing the static coupling-Q of the idler and pump cavity modes at $Q_n = \omega_n/2\kappa_n = 6667$ $(n = i, p)$ and optimizing the success probability for loss rates corresponding to intrinsic

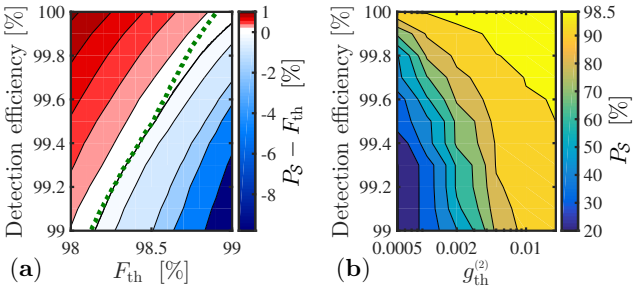

FIG. 4. (a) Difference between the maximum success probability and state fidelity threshold as a function of $F_{\rm th}$ and detection efficiency. The parameters are: $Q_L = 20\times10^7$, $\Delta_i = -\Delta_s = 20\kappa_i$, $\tau_D = 12$ps, $1/\kappa_{\psi_s} = 3$ps, $g^{(2)}_{\rm th} = 1.0$, and $N_{\rm ev} = 3$. The dotted green curve shows the contour corresponding to $\mathcal{P} = F_{\rm th}$ for $N_{\rm ev} = 2$. (b) Success probability as a function of $g^{(2)}_{\rm th}$ and η for $F_{\rm th} = 98.5\%$.

quality factors of 40M, 80M, and 200M. Fig. 4a shows the trade-space between the state fidelity threshold and success probability at different detection efficiency for $Q_L =$ 200M and $g^{(2)}_{\rm th} = 1.0$. Remarkably, a success probability and state fidelity of 99% is achievable for η just below unity. Alternatively, a 99% state fidelity is achieved with $\mathcal{P} = 89.2\%$ if $\eta = 0.99$. Note that $\mathcal{P} > F_{\rm th}$ is possible because some detection sequences result in a state fidelity larger than the threshold. Fig. 4b shows the effect of reducing the second order correlation threshold for $F_{\rm th} = 98.5\%$. It illustrates the reduction in success probability when requiring a lower multi-photon contamination level. We investigated the detrimental effect of increas-

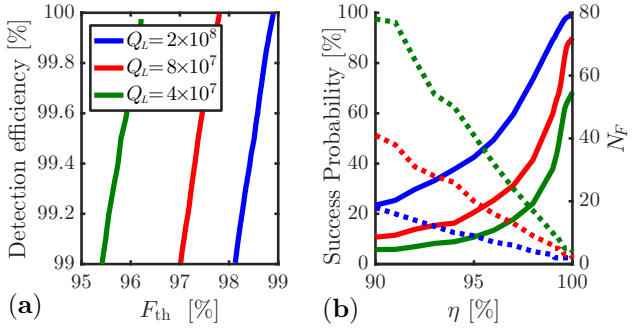

FIG. 5. (a) Contour-lines $\mathcal{P} = F_{\rm th}$ for three different loss rates. (b) Left axis: Success probability as a function of detection efficiency for $F_{\rm th} = 99\%$ (solid lines). Right axis: Number of parallel frequency modes necessary to achieve an efficiency of $\mathcal{P}_{\rm tot} = 99\%$ (dotted lines). The parameters are the same as in Fig. 4 except $N_{\rm ev} = 2$.

ing the loss rate and how performance can be restored using frequency multiplexing. Fig. 5a shows the contour-lines $\mathcal{P} = F_{\rm th}$ for three different values of Q_L. In Fig. 5b we plot the the success probability with $F_{\rm th} = 99\%$ as a function of detection efficiency. Fig. 5b also shows the necessary number of parallel frequency modes to achieve a total success probability of $\mathcal{P}_{\rm tot} = 99\%$. For instance, reducing Q_L from 200M to 40M only requires 4 frequency modes to restore $\mathcal{P}_{\rm tot}$ for $\eta = 1$.

V. DISCUSSION

Our analysis shows that heralded single photon sources should be possible by on-chip multiplexing with near-unity purity. However, the device requirements are stringent - especially on the detector and feed-forward.

State of the art demonstrations of chip-integrated resonators [19–21] have reached quality factors exceeding 200M, showing that the required intrinsic quality factors are within reach. For our protocol, the storage-ring round-trip time should be much shorter than the pump pulse duration. Practically, this means that the storage ring should be less than $\sim 100\mu$m in circumference.

The only detector technology that is currently able to approach the performance requirements are superconducting nanowire single photon detectors (SNSPDs) [22–26]. Electronic logic [27] and electro-optic switching [28] have been demonstrated at cryogenic temperatures, which are necessary when using SNSPDs and assuming a control set-time, τ_D, on the order of 10ps.

As seen from Fig. 4a, the performance is not significantly reduced if the release step is omitted ($N_{\rm ev} = 2$). This means that the tunable signal filter only needs to be low-loss in its closed state since loss during evacuation is irrelevant. In comparison, switches for spatial multiplexing must be low-loss in both states. The tunable output filter must be low-loss in both settings, but it is used only once per emission cycle. One might also consider using two different physical mechanisms to tune $\Delta\psi_s$ and $\Delta\psi_o$, such as carrier dispersion and heating. Developments in reducing the thermal response time in nanophotonic structures [29] could be a path towards high-speed low-loss switching.

Using cavity modes with different coupling rates for the idler, pump, and signal has been shown to enable high-purity states [30]. The main challenges for creating indistinguishable photons with our proposed architecture is stabilization of the high Q resonance and repeatability of the output filter opening. The purity and temporal shaping of photons emitted from our proposed architecture will be studied in more detail in future work.

In conclusion, near-unity efficiency and photon purity is achieved by Bayesian inference, based on known system parameters and photon detections; similar Bayesian state-estimation should also be useful for improving bulk-optics multiplexed sources [6] and relative-multiplexing schemes [31]. This proposal of near-perfect on-chip single photon sources substantiates the feasibility of quantum technologies that require the production of large-scale photonic quantum states, such as optical quantum repeater networks, precision measurements, and quantum computing systems.

ACKNOWLEDGMENTS

MP and DE acknowledge support from AFOSR MURI for Optimal Measurements for Scalable Quantum Technologies (FA9550-14-1-0052) and the Air Force Research Laboratory RITA program (FA8750-14-2-0120). MP acknowledges support from DARPA project Scalable Engineering of Quantum Optical Information Processing Architectures (SEQUOIA), under US Army contract number W31P4Q-15-C-0045 . MH acknowledges support from the Danish Council for Independent Research (DFF1325-00144) and the Villum Foundation.

[1] P. Kok, K. Nemoto, T. C. Ralph, J. P. Dowling, and G. J. Milburn, Reviews of Modern Physics **79**, 135 (2007).

[2] N. Somaschi, V. Giesz, L. De Santis, J. C. Loredo, M. P. Almeida, G. Hornecker, S. L. Portalupi, T. Grange, C. Anton, J. Demory, C. Gomez, I. Sagnes, N. D. L. Kimura, A. Lemaitre, A. Auffeves, A. G. White, L. Lanco, and P. Senellart, Nature Photonics **10** (2016).

[3] X. Ding, Y. He, Z. C. Duan, N. Gregersen, M. C. Chen, S. Unsleber, S. Maier, C. Schneider, M. Kamp, S. Höfling, C.-Y. Lu, and J.-W. Pan, Physical Review Letters **116**, 1 (2016).

[4] I. Aharonovich, D. Englund, and M. Toth, Nature Photonics **10**, 631 (2016).

[5] M. J. Collins, C. Xiong, I. H. Rey, T. D. Vo, J. He, S. Shahnia, C. Reardon, T. F. Krauss, M. J. Steel, a. S. Clark, and B. J. Eggleton, Nature communications **4**, 2582 (2013).

[6] F. Kaneda, B. G. Christensen, J. J. Wong, H. S. Park, K. T. McCusker, and P. G. Kwiat, Optica **2**, 1010 (2015).

[7] B. L. Glebov, J. Fan, and a. Migdall, Applied Physics Letters **103**, 031115 (2013).

[8] C. Joshi, A. Farsi, S. Clemmen, S. Ramelow, and A. Gaeta, in *CLEO Technical Digest* (2016) pp. 4–5.

[9] M. Pant, H. Krovi, D. Englund, and S. Guha, Physical Review A **95**, 012304 (2017).

[10] V. Giovannetti, S. Lloyd, and L. Maccone, Nature Photonics **5**, 222 (2011), arXiv:1102.2318v1.

[11] Y. Li, P. C. Humphreys, G. J. Mendoza, and S. C. Benjamin, Physical Review X **5**, 041007 (2015).

[12] M. Pant, D. Towsley, D. Englund, and S. Guha, arXiv preprint arXiv:1701.03775 (2017).

[13] C. K. Madsen, G. Lenz, A. J. Bruce, M. A. Cappuzzo, L. T. Gomez, and R. E. Scotti, IEEE Photonics Technology Letters **11**, 1623 (1999).

[14] K. Makino, Y. Hashimoto, J.-i. Yoshikawa, H. Ohdan, T. Toyama, P. van Loock, and A. Furusawa, Science Advances **2**, 1 (2016).

[15] A. Li, T. Chen, Y. Zhou, and X. Wang, Optics Letters **41**, 2 (2016).

[16] J. R. Johansson, P. D. Nation, and F. Nori, Computer Physics Communications **184**, 1234 (2013).

[17] Q. Li, M. Davanco, and K. Srinivasan, Nature Photonics **10**, 406 (2016), arXiv:1510.02527.

[18] H. Haus and W. Huang, Proceedings of the IEEE **79**, 1505 (1991).

[19] A. Biberman, M. J. Shaw, E. Timurdogan, J. B. Wright, and M. R. Watts, Optics Letters **37**, 4236 (2012).

[20] K. Y. Yang, D. Y. Oh, S. H. Lee, Q.-F. Yang, X. Yi, and K. Vahala, ArXiv , 1 (2017).

[21] X. Ji, F. A. S. Barbosa, S. P. Roberts, A. Dutt, J. Cardenas, Y. Okawachi, A. Bryant, A. L. Gaeta, and M. Lipson, Optica **4**, 619 (2017), arXiv:1609.08699.

[22] A. Divochiy, F. Marsili, D. Bitauld, A. Gaggero, R. Leoni, F. Mattioli, A. Korneev, V. Seleznev, N. Kaurova, O. Minaeva, G. Gol'tsman, K. G. Lagoudakis, M. Benkhaoul, F. Lévy, and A. Fiore, Nature Photonics **2**, 302 (2008), arXiv:0712.3080.

[23] F. Marsili, V. B. Verma, J. a. Stern, S. Harrington, a. E. Lita, T. Gerrits, I. Vayshenker, B. Baek, M. D. Shaw, R. P. Mirin, and S. W. Nam, Nature Photonics **7**, 210 (2013).

[24] C. Schuck, W. H. P. Pernice, and H. X. Tang, Scientific Reports **3**, 1893 (2013), arXiv:1306.0164.

[25] F. Najafi, J. Mower, N. C. Harris, F. Bellei, A. Dane, C. Lee, X. Hu, P. Kharel, F. Marsili, S. Assefa, K. K. Berggren, and D. Englund, Nature Communications **6**, 5873 (2015).

[26] E. Schelew, M. K. Akhlaghi, and J. F. Young, Nature Communications **6**, 1 (2015).

[27] A. N. McCaughan and K. K. Berggren, Nano letters **14**, 5748 (2014).

[28] M. Gehl, C. Long, D. Trotter, A. Starbuck, A. Pomerene, J. B. Wright, S. Melgaard, J. Siirola, A. L. Lentine, and C. DeRose, Optica **4**, 374 (2017).

[29] J. B. Khurgin, G. Sun, W. T. Chen, W.-Y. Tsai, and D. P. Tsai, Scientific reports **5**, 17899 (2015).

[30] Z. Vernon, M. Menotti, C. C. Tison, J. A. Steidle, M. L. Fanto, P. M. Thomas, S. F. Preble, A. M. Smith, P. M. Alsing, M. Liscidini, and J. E. Sipe, arXiv , 1 (2017), arXiv:1703.10626.

[31] M. Gimeno-segovia, H. Cable, G. J. Mendoza, P. Shadbolt, J. W. Silverstone, J. Carolan, M. G. Thompson, J. L. O' Brien, and T. Rudolph, New Journal of Physics **19** (2017).

SUPPLEMENTAL MATERIAL: TEMPORALLY AND FREQUENCY MULTIPLEXED SINGLE PHOTON SOURCE USING QUANTUM FEEDBACK CONTROL FOR SCALABLE PHOTONIC QUANTUM TECHNOLOGIES

I. DEVICE ARCHITECHTURE

Our proposed device implementation uses a photonic integrated circuit consisting of a ring resonator and MZI-couplers [S1], as illustrated in Fig. 1 of the main text. Here, we analyze this structure in more detail. The structure is shown again in Fig. S1 with definitions of fields used in the analysis. The outputs of the MZI filters are

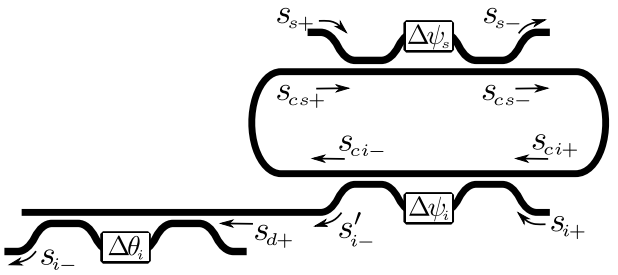

FIG. S1. Device architecture including definitions of fields used in the analysis. Note that the output filter is omitted.

related to the inputs by

$$\begin{bmatrix} s_{n-} \\ s_{cn-} \end{bmatrix} = \mathbf{C}^{(n)}\mathbf{Z}^{(n)}\mathbf{C}^{(n)} \begin{bmatrix} s_{n+} \\ s_{cn+} \end{bmatrix},\ n=\{i,s\} \tag{S1}$$

where $\{i,s\}$ represent the idler and signal filter. The matrices $\mathbf{C}^{(n)}$ and $\mathbf{Z}^{(n)}$ are given by

$$\mathbf{C}^{(n)}=\begin{bmatrix} \nu & \mathrm{i}\sqrt{1-\nu^2} \\ \mathrm{i}\sqrt{1-\nu^2} & \nu \end{bmatrix},\ \mathbf{Z}^{(n)}=\begin{bmatrix} e^{\mathrm{i}\psi_{nT}} & 0 \\ 0 & e^{\mathrm{i}\psi_{nB}} \end{bmatrix}, \tag{S2}$$

where ψ_{nT} and ψ_{nB} are the phase accumulation in the upper and lower arm of the MZI and ν describes the through-coupling of the waveguide couplers. The transfer matrix $\mathbf{T}^{(n)}=\mathbf{C}^{(n)}\mathbf{Z}^{(n)}\mathbf{C}^{(n)}$ of the MZI filter is

$$\mathbf{T}^{(n)}=e^{\mathrm{i}\psi_{nB}}\begin{bmatrix} (1+e^{\mathrm{i}\psi_n})\nu^2-1 & \mathrm{i}(1+e^{\mathrm{i}\psi_n})\nu\sqrt{1-\nu^2} \\ \mathrm{i}(1+e^{\mathrm{i}\psi_n})\nu\sqrt{1-\nu^2} & \nu^2-e^{\mathrm{i}\psi_n}(1-\nu^2) \end{bmatrix}, \tag{S3}$$

where $\psi_n=\psi_{nT}-\psi_{nB}$ is the difference in phase accumulation between the two arms. We assume that the phases $\Delta\psi_n$ are tunable such that

$$\psi_n(\omega)=k(\omega)\Delta L_n+\Delta\psi_n,\ n=\{i,s\}. \tag{S4}$$

The path length difference between the MZI arms is ΔL_n and the propagation constant is approximated as

$$k(\omega)\approx\frac{\tilde{n}_{\mathrm{eff}}}{c}\omega_0+\frac{n_g}{c}(\omega-\omega_0). \tag{S5}$$

The complex effective mode index is $\tilde{n}_{\mathrm{eff}}=n'_{\mathrm{eff}}+\mathrm{i}n''_{\mathrm{eff}}$ and the group index is defined from $n_g/c\equiv\partial k/\partial\omega$.

To analyze the structure in Fig. S1, let us consider a situation where a field, s_f, is generated inside the ring between the signal and idler filter, such that

$$s_{ci+}=e^{\mathrm{i}\phi_{si}}s_{cs-}+s_f \tag{S6}$$
$$s_{s+}=s_{i+}=0. \tag{S7}$$

The fields are then related using Fig. S1

$$\begin{aligned} s_{ci+}=e^{\mathrm{i}\phi_{si}}T^{(s)}_{2,2}s_{cs+}+s_f\ &= \\ e^{\mathrm{i}\phi_{si}}T^{(s)}_{2,2}e^{\mathrm{i}\phi_{is}}s_{ci-}+s_f\ &= \\ e^{\mathrm{i}\phi_{si}}T^{(s)}_{2,2}e^{\mathrm{i}\phi_{is}}T^{(i)}_{2,2}s_{ci+}+s_f,& \end{aligned} \tag{S8a}$$

where $T^{(n)}_{i,j}$ is the matrix element of $\mathbf{T}^{(n)}$ corresponding to the ith row and jth column. The round-trip phase of the isolated storage ring is

$$\phi_c(\omega)=\psi_{iB}+\phi_{is}+\psi_{sB}+\phi_{si}=k(\omega)L_c, \tag{S9}$$

where L_c is the length of the storage ring. From Eq. (S8a), we have

$$s_{ci+}=\frac{1}{1-e^{\mathrm{i}\phi_c}\zeta_i\zeta_s}s_f, \tag{S10}$$

where we defined the tuning parameter

$$\zeta_n\equiv\nu^2-e^{\mathrm{i}\psi_n}(1-\nu^2). \tag{S11}$$

The out-going fields are given by

$$s_{s-}=T^{(s)}_{1,2}s_{cs+}=\frac{T^{(s)}_{1,2}e^{\mathrm{i}\phi_{is}}T^{(i)}_{2,2}}{1-e^{\mathrm{i}\phi_c}\zeta_i\zeta_s}s_f \tag{S12a}$$

$$s_{i-}=D^{(i)}_{1,2}s'_{i-}=\frac{D^{(i)}_{1,2}T^{(i)}_{1,2}}{1-e^{\mathrm{i}\phi_c}\zeta_i\zeta_s}s_f. \tag{S12b}$$

The drop filter transfer matrix is

$$\mathbf{D}^{(i)}=e^{\mathrm{i}\theta_{iB}}\frac{1}{2}\begin{bmatrix} e^{\mathrm{i}\theta_i}-1 & \mathrm{i}(1+e^{\mathrm{i}\theta_i}) \\ \mathrm{i}(1+e^{\mathrm{i}\theta_i}) & 1-e^{\mathrm{i}\theta_i} \end{bmatrix}. \tag{S13}$$

We chose $\nu=1/\sqrt{2}$ to achieve 100% visibility of the drop filter and as in Eq. (S4), the phase difference between the arms is

$$\theta_i(\omega)=k(\omega)\Delta L_{di}+\Delta\theta_i. \tag{S14}$$

The idler, pump, and signal frequencies are chosen from three adjacent modes of the storage ring, such that

$$\omega_i=\omega_p-\Omega_c,\qquad \omega_s=\omega_p+\Omega_c, \tag{S15}$$

where Ω_c is the free spectral range (FSR) of the storage ring

$$\Omega_c=\frac{2\pi c}{n_gL_c}. \tag{S16}$$

From the out-coupling matrix elements

$$T^{(n)}_{1,2}=e^{\mathrm{i}\psi_{nB}}\mathrm{i}(1+e^{\mathrm{i}\psi_n})\nu\sqrt{1-\nu^2}, \tag{S17}$$

it is observed that frequencies corresponding to $\psi_n(\omega) = \pi + 2\pi p$ can not pass through the filters. This fact is used to realize a way to obtain the desired properties of the filters:

$$\psi_i(\omega_i) = 2\pi, \qquad \psi_i(\omega_s) = \pi \tag{S18a}$$
$$\psi_s(\omega_s) = \pi, \qquad \psi_s(\omega_i) = \pi \tag{S18b}$$
$$\theta_i(\omega_i) = 2\pi, \qquad \theta_i(\omega_p) = \pi. \tag{S18c}$$

The conditions in Eq. (S18) can be met by making the FSRs of the filters different integer values of Ω_c. Correspondingly, the path length differences should be different integer fractions of L_c as

$$\Delta L_i = L_c/4, \quad \Delta L_{di} = L_c/2, \quad \Delta L_s = L_c. \tag{S19}$$

In Fig. S2 we plot the output fields (top panel) and the field circulating inside the storage ring (bottom panel) for these choices. From the top panel it is seen that $|s_{i-}|^2$ vanishes at ω_p and ω_s, and $|s_{s-}|^2$ goes to zero at ω_i, ω_p, and ω_s. From the bottom panel of Fig. S2, it is

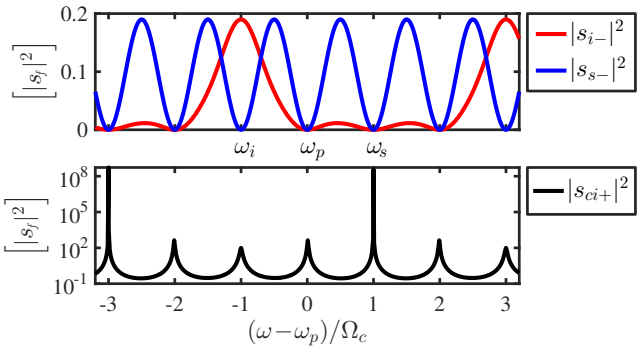

FIG. S2. Top: Output fields, $|s_{n-}|^2/|s_f|^2$, as a function of frequency. Bottom: Circulating field $|s_{ci+}|^2/|s_f|^2$ as a function of frequency. Parameters: $\nu^2 = 0.95$, $L_c = 100\mu$m, $n''_{\text{eff}} = 10^{-7}$, $n'_{\text{eff}} = 2.5$, and $n_g = 4$.

observed that the signal mode at ω_s is spectrally narrow compared to the idler and pump modes. This is caused by the choice $\psi_s(\omega_s) = \pi$, which corresponds to the signal filter being closed and the Q-factor only being limited by intrinsic loss.

The signal filter is tuned by modifying $\Delta\psi_s$. The corresponding change in the cavity-waveguide coupling is found from the tunability parameter ζ_s. Comparing Eqs. (S3) and (S11) it is seen that ζ_s describes the loss per round trip of the intra-cavity field due to waveguide coupling. A coupling rate may therefore be defined by the relation

$$\exp\left[-\kappa_n \tau_{\text{RT}}\right] = |\zeta_n|, \tag{S20}$$

where τ_{RT} is the cavity round-trip time. The coupling rate is

$$\kappa_n(\omega, \Delta\psi_n) = -\frac{c}{n_g L_c} \ln\left[|\zeta_n(\omega, \Delta\psi_n)|\right]. \tag{S21}$$

The resonances, ω_n, of the MZI-coupled ring are also affected by tuning $\Delta\psi_s$. They are found by the resonance condition on the round-trip phase of the MZI-coupled ring

$$\Phi_n(\omega_n) = \phi_c(\omega_n) + \arg\left[\zeta_i(\omega_n)\zeta_s(\omega_n)\right] = 2\pi. \tag{S22}$$

In Fig. S3 we plot the coupling rate and resonance shift

$$\delta_s(\psi_s) = \omega_s(\psi_s) - \omega_s(\psi_s = \pi) \tag{S23}$$

as a function of ψ_s. The coupling rate remains finite at $\psi_s = \pi$ due to the small imaginary part of the complex refractive index.

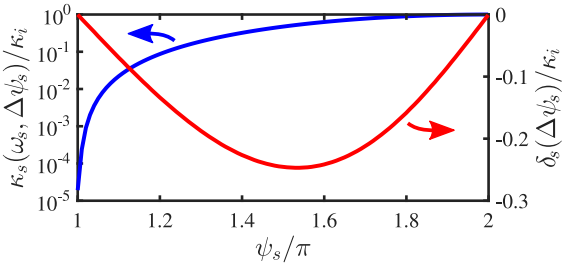

FIG. S3. Coupling rate and resonance shift as a function of ψ_s. Both curves are normalized by the static coupling rate through the idler filter, $\kappa_i(\omega_i)$. Parameters are the same as in Fig. S2.

If the tunable phase, $\Delta\psi_s(t)$, has some time variation due to the electrical signal coming from the logic unit (see Fig. 1 of the main text), the coupling rate will also vary in time, $\kappa_s(t)$. The interference-based filtering of the MZI will work as long as $\Delta\psi_s(t)$ varies slowly relative to the propagation time through the MZI. We ignore the resonance shift, δ_s, when modeling the dynamics of the storage ring by assuming that the chirp it induces on the signal photon does not affect its detection.

The analysis above shows that we can model the system using a time-dependent coupling rate for the signal mode.

A. Frequency conversion

We note that with the choices of ΔL_n made here, we could in principle use any mode-pair satisfying

$$\omega_s = \omega_p + \Omega_c(1+4p), \ \omega_i = \omega_p - \Omega_c(1+4p), \ p \in \mathbb{Z}_0. \tag{S24}$$

This architecture therefore lends itself naturally to be used for temporal- and frequency multiplexing in parallel. However, if Bragg-Scattering FWM [S2] is used, the probability of up-conversion and down-conversion of the signal photon is equal (provided that phase-matching is uniform across several FSRs of the storage ring) [S3, S4]. To overcome this symmetry, the storage ring can be coupled

to an auxiliary ring with a length $L_r = L_c/16$ such that its resonances coincide with every fourth signal mode. The ring-ring coupling will cause a splitting of the mode spectrum and thereby effectively eliminate either the up- or down-conversion cavity mode. To illustrate this, let us consider the auxiliary ring being coupled on the left side of the storage ring with a coupling region described by a matrix $\mathbf{C}^{(a)}$ as in Eq. (S2). The relation between s_{cs+} and s_{ci-} then becomes

$$s_{cs+} = \xi s_{ci-} + \mathrm{i}\sqrt{1-\xi^2}\, s_{a+} \tag{S25a}$$

$$s_{a-} = \mathrm{i}\sqrt{1-\xi^2}\, s_{ci-} + \xi s_{a+} \tag{S25b}$$

$$s_{a+} = e^{\mathrm{i}\phi_a} s_{a-}, \tag{S25c}$$

where ξ is the coupling strength, s_{a-} is the field in the auxiliary ring moving away from the coupling region, s_{a+} is the corresponding field moving towards the coupling region, and ϕ_a is the round-trip phase of the auxiliary ring. Solving Eq. (S25) gives

$$s_{cs+} = \left(\xi - \frac{(1-\xi^2)e^{\mathrm{i}\phi_a}}{1-\xi e^{\mathrm{i}\phi_a}}\right) s_{ci-}. \tag{S26}$$

Following the calculation in Eq. (S8) and inserting Eq. (S26) yields a modified version of Eq. (S10)

$$s_{ci+} = \frac{1}{1 - e^{\mathrm{i}\phi_c}\zeta_i\zeta_s\left(\xi - \frac{(1-\xi^2)e^{\mathrm{i}\phi_a}}{1-\xi e^{\mathrm{i}\phi_a}}\right)} s_f. \tag{S27}$$

In Fig. S4 we show the circulating field with- and without the auxiliary ring coupled. Notice the splitting of the

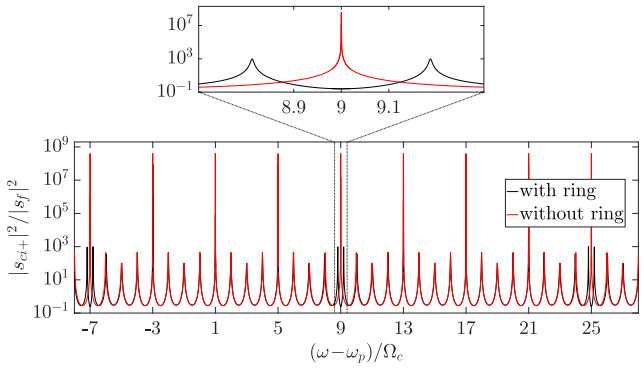

FIG. S4. Power spectrum of the circulating field in the storage ring with- (black) and without (red) an auxiliary coupled ring. Parameters are the same as in Fig. S2, and $\xi^2 = 0.9$.

cavity modes at the blocked frequencies

$$\omega_{\mathrm{block}} = \omega_p + \Omega_c(9+16p),\ p \in \mathbb{Z}_0. \tag{S28}$$

Detecting an idler photon at e.g. $\omega_i = \omega_p - 5\Omega_c$ heralds the presence of a signal photon at $\omega_s = \omega_p + 5\Omega_c$. Since the mode at $\omega_p + 9\Omega_c$ is now eliminated, the signal can be down-converted to the target frequency $\omega_p + \Omega_c$ with high efficiency. In general, we can frequency-multiplex using all signal modes satisfying the relation

$$\omega_s = \omega_p + \Omega_c(5+8p),\ p \in \mathbb{Z}_0. \tag{S29}$$

The fact that the signal photon is born inside the storage cavity (as opposed to the situation in Refs. [S3, S5]) significantly simplifies the problem and near-unity conversion efficiency should be possible [S4, S6].

II. PROBABILITY ANALYSIS

We repeat the threshold conditions for reference

$$P(n^{(M)} = 1 | \boldsymbol{d}^{(M^*)}) \geq F_{\mathrm{th}} \quad \textit{and} \quad g^{(2)}(\boldsymbol{d}^{(M^*)}) \leq g^{(2)}_{\mathrm{th}}. \tag{S30}$$

The probability $P(n^{(m)}, \boldsymbol{d}^{(m^*)})$ is evaluated using an expansion

$$P(n^{(m)}, \boldsymbol{d}^{(m^*)}) = \sum_{n^{(m-1)}} P(n^{(m)}, n^{(m-1)}, \boldsymbol{d}^{(m^*)}) = \sum_{n^{(m-1)}} P(n^{(m)}, d^{(m^*)} | n^{(m-1)}, \boldsymbol{d}^{(m-1)}) P(n^{(m-1)}, \boldsymbol{d}^{(m-1)}). \tag{S31}$$

Notice that the probability distribution in the current bin m is updated using information from the total duration of the previous bins, $\boldsymbol{d}^{(m-1)}$, because the detector keeps acquiring information until the end of each bin. The second factor on the right-hand side (RHS) of Eq. (S31) is found by a similar expansion, which means that the distribution $P(n^{(m)}, \boldsymbol{d}^{(m^*)})$ can be found iteratively starting from the first bin

$$P(n^{(1)}, \boldsymbol{d}^{(1)}) = \sum_{n^{(0)}} P(n^{(1)}, d^{(1)} | n^{(0)}, d^{(0)}) P(n^{(0)}, d^{(0)}), \tag{S32}$$

where $P(n^{(0)}, d^{(0)})$ is known since $n^{(0)}$ and $d^{(0)}$ both equal zero at the beginning of each emission cycle. Note that we omit an expansion over the initial state of the idler mode in Eq. (S31) by assuming that it is in the vacuum state. In the following sections, it is explained how the probability distributions $P(n^{(m)}, d^{(m)} | n^{(m-1)}, \boldsymbol{d}^{(m-1)})$ and $P(n^{(m)}, d^{(m^*)} | n^{(m-1)}, \boldsymbol{d}^{(m-1)})$ are calculated for pumping and releasing, respectively.

A. Pump model

If the cavity is pumped in bin m, the probability that there are $n^{(m)}$ signal photons in the cavity *and* the detection number is $d^{(m)}$ at t_m is

$$P_p(n^{(m)}, d^{(m)} | n^{(m-1)}, \boldsymbol{d}^{(m-1)}) = \sum_{n_i^{(m)} = I^{(m)}}^{\infty} P(d^{(m)} | n_i^{(m)}) P_p(n^{(m)}, n_i^{(m)} | n^{(m-1)}, \boldsymbol{d}^{(m-1)}), \tag{S33}$$

where $n_i^{(m)}$ is the number of idler photons coupled through the idler filter between t_{m-1} and t_m. The subscript p is used to signify that we pump in bin m. The number of detected idler photons is $I^{(m)} = d^{(m)} - d^{(m-1)}$, because the signal filter is closed so no signal detections contribute to $d^{(m)}$. Note that the probability of $d^{(m)}$ only depends on $n_i^{(m)}$ and is given by

$$P(d^{(m)}|n_i^{(m)}) = \binom{n_i^{(m)}}{I^{(m)}} \eta^{I^{(m)}} (1-\eta)^{n_i^{(m)}-I^{(m)}}, \tag{S34}$$

where η is the detection efficiency. The distribution $P_p(n^{(m)}, d^{(m^*)}|n^{(m-1)}, \boldsymbol{d}^{(m-1)})$ is found by replacing $d^{(m)}$, $n_i^{(m)}$, and $I^{(m)}$ by $d^{(m^*)}$, $n_i^{(m^*)}$, and $I^{(m^*)}$ in Eqs. (S33) and (S34).

To calculate the probability $P_p(n^{(m)}, n_i^{(m)}|n^{(m-1)}, \boldsymbol{d}^{(m-1)})$, the system is modeled by the Hamiltonian

$$H_{sys} = \Delta_i \hat{a}_i^\dagger \hat{a}_i + \Delta_s \hat{a}_s^\dagger \hat{a}_s + \mathcal{X}\big(\hat{a}_i^\dagger \hat{a}_s^\dagger + \hat{a}_i \hat{a}_s\big), \tag{S35}$$

where $\hat{a}_s$ and $\hat{a}_i$ are annihilation operators of the signal and idler modes, respectively. We use normalized units ($\hbar = 1$) and a classical pump rate described by $\mathcal{X}$, which is proportional to the nonlinear coefficient, $\chi^{(3)}$, and the energy of the pump mode. Δ_s and Δ_i are the detunings between the pump frequency and the signal and idler, respectively. Coupling between the resonator and waveguides through the filters is modeled via collapse operators, $\hat{C}_{nL} = \sqrt{2\kappa_L}\hat{a}_n$, and $\hat{C}_n = \sqrt{2\kappa_n}\hat{a}_n$ with $n = i, s$ [S7]. The loss rate, κ_L, of all modes is assumed equal. From coupled mode theory [S8], the pump rate is

$$\mathcal{X}(t) = \left| \int_{-\infty}^{t} e^{-\kappa_p (t-t')} S_{\text{pump}}(t') dt' \right|^2, \tag{S36}$$

where the input power is $|S_{\text{pump}}(t)|^2 \propto \exp[-(t-t_p)^2/\tau_p^2]$. The pump width τ_p is 1ps and the time t_p is adjusted such that $\mathcal{X}(t_{m-1})$ is at least a thousand times smaller than its maximum.

The state of the storage ring, $|\psi(t)\rangle$, is calculated from Eq. (S35) using a Monte Carlo method [S7] with an initial state $|n^{(m-1)}, n_{ci}^{(m-1)} = 0\rangle$. The assumption of zero idler photons at t_{m-1} is based on the coupling rate, κ_i, being much larger than the inverse bin duration, $1/\tau_{\text{bin}}$. Since we only consider near-unity detection efficiency, we assume that the probability $P_p(n^{(m-1)} > 2|d^{(m^*-1)} \leq 0)$ is negligible and therefore truncate the summation in Eq. (S31) after 2 for bins where we pump. The probability of a certain configuration with $n^{(m)}$ photons in the signal mode and $n_i^{(m)}$ idler photons in the detector waveguide is found by projecting the state $|n^{(m)}, n_{ci}^{(m)}\rangle$ onto $|\psi(t_m)\rangle$ and tracing out the idler subspace for all Monte Carlo trajectories, where $n_i^{(m)}$ idler photons couple into the detector waveguide

$$P_p(n^{(m)}, n_i^{(m)}|n^{(m-1)}, \boldsymbol{d}^{(m-1)}) = \sum_{\text{traj}(n_i^{(m)})} \sum_{n_{ci}^{(m)}} \frac{\left|\langle n^{(m)}, n_{ci}^{(m)}|\psi(t_m)\rangle\right|^2}{N_{\text{traj}}}. \tag{S37}$$

Note that the probability is obtained by normalizing with the total number of trajectories N_{traj}. The probability $P_p(n^{(m)}, n_i^{(m^*)}|n^{(m-1)}, \boldsymbol{d}^{(m-1)})$ is found by counting the number of idler collapses up until the time t_{m^*} instead of t_m.

With the time dependence of $|S_{\text{pump}}(t)|^2$ fixed, we can introduce the probability that at least one pair is created in bin m, $p^{(m)}$, as a generalized control setting for the pump. It is calculated using Monte Carlo simulations with the initial condition $|\psi(t_{m-1})\rangle = |0, 0\rangle$.

B. Release model

If we release signal photons in bin m, the probability distribution $P_r(n^{(m)}, d^{(m)}|n^{(m-1)}, \boldsymbol{d}^{(m-1)})$ is also found using Eqs. (S33) and (S34) with $I^{(m)}$ and $n_i^{(m)}$ replaced by $S^{(m)}$ and $n_s^{(m)}$, where $S^{(m)} = d^{(m-1)} - d^{(m)}$. Again, the subscript r indicates that we are releasing signal photons in bin m. The probability of different cavity states at t_m is given by the multinomial distribution

$$P_r(n^{(m)}, n_s^{(m)}|n^{(m-1)}, \boldsymbol{d}^{(m-1)}) = \frac{n^{(m-1)}!\, p_c^{n^{(m)}} p_s^{n_s^{(m)}} p_L^{n^{(m-1)} - n_s^{(m)} - n^{(m)}}}{n_s^{(m)}!\, n^{(m)}!\, (n^{(m-1)} - n_s^{(m)} - n^{(m)})!}, \tag{S38}$$

Using rate equations for the ensemble average of the number operators

$$\frac{d\langle \hat{n}_c(t)\rangle}{dt} = -\big[\kappa_s(t) + \kappa_L\big]\langle \hat{n}_c(t)\rangle \tag{S39a}$$

$$\frac{d\langle \hat{n}_s(t)\rangle}{dt} = 2\kappa_s(t)\langle \hat{n}_c(t)\rangle \tag{S39b}$$

$$\frac{d\langle \hat{n}_L(t)\rangle}{dt} = 2\kappa_L\langle \hat{n}_c(t)\rangle, \tag{S39c}$$

the probabilities on the RHS of Eq. (S38) are found by, e.g. $\langle \hat{n}_c\rangle = n^{(m-1)} p_c$. The subscripts $\{c, s, L\}$ correspond to the cavity, signal waveguide, and loss channel, respectively. With the initial condition: $p_c(t_{m-1}) = 1$ and $p_s(t_{m-1}) = p_L(t_{m-1}) = 0$, the solution to Eq. (S39) is

$$p_c(t) = \exp\left(\int_{t_{m-1}}^{t} -2\big[\kappa_s(t') + \kappa_L\big]dt'\right) \tag{S40a}$$

$$p_s(t) = \int_{t_{m-1}}^{t} 2\kappa_s(t') p_c(t') dt' \tag{S40b}$$

$$p_L(t) = \int_{t_{m-1}}^{t} 2\kappa_L p_c(t') dt'. \tag{S40c}$$

The distribution $P_r(n^{(m)}, n_s^{(m^*)}|n^{(m-1)}, \boldsymbol{d}^{(m-1)})$ is found using the intermediary step

$$P_r(n^{(m)}, n_s^{(m^*)}|n^{(m-1)}, \boldsymbol{d}^{(m-1)}) = \sum_{n^{(m^*)}, n_s^{(m)}} P_r(n^{(m)}, n_s^{(m)}|n^{(m^*)}, n_s^{(m^*)}, n^{(m-1)}, \boldsymbol{d}^{(m-1)}) \times P_r(n^{(m^*)}, n_s^{(m^*)}|n^{(m-1)}, \boldsymbol{d}^{(m-1)}), \tag{S41}$$

where the first factor on the RHS only depends on $n^{(m^*)}$, such that

$$P_r(n^{(m)}, n_s^{(m^*)}|n^{(m-1)}, \boldsymbol{d}^{(m-1)}) = \sum_{n^{(m^*)}, n_s^{(m)}} P_r(n^{(m)}, n_s^{(m)}|n^{(m^*)}) P_r(n^{(m^*)}, n_s^{(m^*)}|n^{(m-1)}, \boldsymbol{d}^{(m-1)}). \quad \text{(S42)}$$

The distribution $P_r(n^{(m)}, n_s^{(m)}|n^{(m^*)})$ must be evaluated using Eqs. (S38) and (S40) with the chosen temporal evolution of $\kappa_s(t)$.

We note that Eq. (S40c) shows how $p_c(t)$ should ideally drop instantly from 1 at t_{m-1} to its final value to minimize the risk of loosing a signal photon. This corresponds to $\kappa_s(t)$ being proportional to a Dirac delta distribution centered at t_{m-1}. However, we assume a specific temporal shape given by

$$\kappa_s(t) \propto \int_{t_{m-1}}^{t} e^{-\kappa_{\psi_s}(t-t')} e^{-(t'-t_r)^2/\tau_r^2} dt'. \quad \text{(S43)}$$

where $1/\kappa_{\psi_s}$ is a response time, t_r is adjusted such that $\kappa_s(t_{m-1})$ is at least a thousand times smaller than its maximum and the width, τ_r, is constrained by the condition $\kappa_s(t) \leq \kappa_i$ seen in Fig. S3. With the shape of $\kappa_s(t)$ given by Eq. (S43), the release control setting is completely determined by the value $p_c^{(m)} = p_c(t_m)$ calculated from Eq. (S40a).

III. PROTOCOL

To determine whether to store the current state, we check if it will evolve into a distribution, $P_s(n^{(M)} = 1|\boldsymbol{d}^{(m^*)})$, that meets the criteria in Eq. (S30). It is given by

$$P_s(n^{(M)}|\boldsymbol{d}^{(m^*)}) = \sum_{n^{(m)}=n^{(M)}}^{\infty} P_s(n^{(M)}|n^{(m)}, \boldsymbol{d}^{(m^*)}) P(n^{(m)}|\boldsymbol{d}^{(m^*)}), \quad \text{(S44)}$$

where the subscript s indicates storage until t_M. The first factor on the RHS of Eq. (S44) is given by Eq. (S38) with $p_s = n_s = 0$

$$P_s(n^{(M)}|n^{(m)}, \boldsymbol{d}^{(m)}) = \frac{n^{(m)}! p_c^{n^{(M)}} (1-p_c)^{n^{(m)}-n^{(M)}}}{n^{(M)}! (n^{(m)} - n^{(M)})!}, \quad \text{(S45)}$$

where $p_c = \exp[-2\kappa_L(t_M - t_m)]$ is the probability that a photon remains in the cavity until t_M.

A. Pumping protocol

When pumping in bin m, we assume that it is advantageous to keep the pump power below a level, which for the initial condition $|\psi(t_{m-1})\rangle = |0,0\rangle$ results in a distribution $P_s(n^{(M)} = 1|\boldsymbol{d}^{(m^*)})$ that obeys the requirements in Eq. (S30). Fig. S5 shows how the relevant properties of the distribution $P(n^{(m)}|d^{(m^*)})$ vary as a function of the control setting, $p^{(m)}$, and bin duration, τ_{bin}. For small τ_{bin}, our state estimation fidelity is degraded by the finite probability that idler photons remain inside the cavity. As the bin duration is increased, the fidelity eventually becomes dominated by the detection efficiency and the contours become vertical. This suggests that there must be an optimum bin duration, because increasing it allows larger pump power while reducing the total number of bins. The properties illustrated in Fig. S5 apply to any bin, but since $P_s(n^{(M)}|\boldsymbol{d}^{(m^*)})$ depends on $M-m$, the maximum control setting for the pump must be evaluated for each bin.

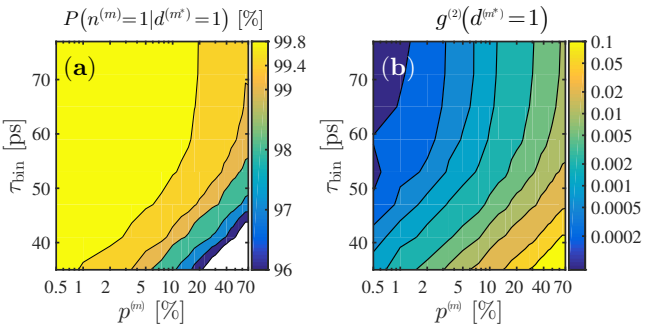

FIG. S5. Conditional probability (a) and second-order correlation (b) after pumping in bin m as a function of the pair creation probability and bin duration. The parameters are: $Q_L = 200\text{M}$, $Q_p = Q_i = 6667$, $\Delta_s = -\Delta_i = 20\kappa_p$, $\eta = 0.996$, $\tau_D = 12\text{ps}$, $|\psi(t_{m-1})\rangle = |0,0\rangle$.

B. Release protocol

To test whether releasing in bin m can lead to a successful state creation, Eq. (S30) can be evaluated using Eq. (S44) for all possible outcomes $\{n^{(m)}, d^{(m^*)}\}$ with a fixed control setting $p_c^{(m)}$. If Eq. (S30) can be fulfilled, the control setting is adjusted to maximize the success probability. Since we are only interested in the high detection efficiency regime, we assume that only $d^{(m^*)} = 1$ provides a sufficiently large state fidelity and therefore only use the outcomes $\{n^{(m)}, 1\}$ to optimize the control setting. If Eq. (S30) can not be met, the cavity is evacuated. Determining whether it is advantageous to release or evacuate requires an evaluation of the success probability for a very large number of outcome scenarios. We therefore simplify the release protocol by always evacuating if $d^{(m^*-1)} \geq N_{\text{ev}}$.

While the optimization procedure described above is done numerically, insight into the maximum success probability of the release process may be gained by considering the probability that $n^{(m+1)} = 1$ after releasing in

bin $m+1$. It is given by Eq. (S38)

$$P(1|n^{(m)},\boldsymbol{d}_r^{(m^*)}) = \sum_{n_s^{(m)}=0}^{n^{(m)}-1} \frac{n^{(m)}! p_c p_s^{n_s^{(m)}} p_L^{n^{(m)}-1-n_s^{(m)}}}{n_s^{(m)}!(n^{(m)}-1-n_s^{(m)})!} =$$
$$n^{(m)} p_c \sum_{n_s^{(m)}=0}^{n^{(m)}-1} \binom{n^{(m)}-1}{n_s^{(m)}} p_s^{n_s^{(m)}} p_L^{n^{(m)}-1-n_s^{(m)}} =$$
$$n^{(m)} p_c (p_s+p_L)^{n^{(m)}-1} = n^{(m)} p_c (1-p_c)^{n^{(m)}-1}. \quad \text{(S46)}$$

The maximum is found when $n^{(m)}p_c = 1$ and equals $1/2$ for $n^{(m)}=2$ and $4/9$ for $n^{(m)}=3$.

C. Optimization of protocol

To optimize our protocol, we start by assuming there is only a single mode available, $M=1$. In this case, pumping is the only choice and the pair creation probability, $p^{(1)}$, is chosen to maximize the success probability while obeying the requirements in Eq. (S30). Next, we assume two modes are available. Again, we pump in the first bin and our action in the second bin depends on $d^{(1^*)}$ as described above. For $M=3$, there is a possibility that $d^{(1^*)}$ causes us to evacuate the cavity in bin 2. In this scenario, we treat the last bin as the $M=1$ case because the initial condition of bin 3 will be $|\psi(t_2)\rangle = |0,0\rangle$. The protocol parameters for the last bin are then set as the optimum parameters found for $M=1$.

For any M, we use a fixed pump sequence $\boldsymbol{p}^{(M)} = \{p^{(1)}, p^{(2)}, \ldots, p^{(M-1)}, p^{(M)}\}$ for all detection sequences that do not result in evacuation in some intermediary bin $m<M$. If evacuation is warranted in bin m, the pump sequence for the remaining M–m bins is chosen as the optimum sequence found for $M-m$ bins. The contribution to the overall success probability is $P(\boldsymbol{d}^{(m^*-1)})\mathcal{P}(M-m)$, where $\boldsymbol{d}^{(m^*-1)}$ is the detection sequence leading us to evacuate in bin m.

The success probability is maximized by adjusting the pair creation probabilities in the pump sequence using the discrete set of values [0.1, 0.2, 0.5, 1, 2, 3.5, 5:2.5:50, 55, 60, 65, 70] (in %) for which the single bin probability distribution in Eq. (S37) has been found using Monte Carlo simulations. Fig. S6 shows an example of the optimized pump sequences. For each M on the horizontal axis, the vertical axis plots the sequence $\boldsymbol{p}^{(m)}$ with colors indicating the value of $p^{(m)}$. For $M > 20$, the cavity is always evacuated in a bin m, for which $m < M$. For $M > 25$, the optimum strategy is to evacuate at $m = m_{\text{ev}}$ and the number of colored bins is given by $m_{\text{ev}} - 1$. As the number of possible pump sequences increases exponentially with M, we optimize using a small sample of bins and then use linear interpolation to find $p^{(m)}$ for all bins. The black dots indicate which bins are used in the interpolation.

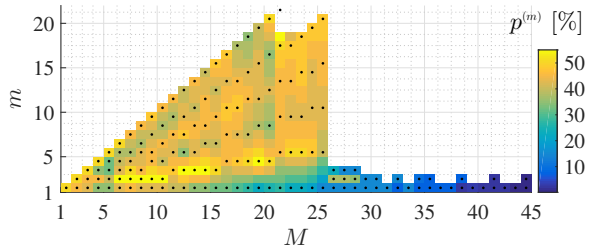

FIG. S6. Optimized probabilities of creating at least one photon pair as a function of m for different lengths of the emission cycle, M. The black dots indicate bins used for linear interpolation. The parameters are: $Q_L = 200\text{M}$, $\eta = 0.996$, $F_{th} = 0.985$, $g^{(2)}_{\text{th}} = 1.0$, $N_{\text{ev}} = 3$.

The values of F_{ev} corresponding to the optimization example in Fig. S6 are plotted in Fig. S7.

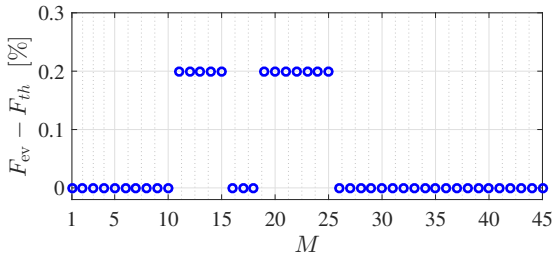

FIG. S7. Optimum values of F_{ev} as a function of M corresponding to the optimization in Fig. S6.

Finally, we also show how the optimized success probability depends on the bin duration in Fig. S8. The optimum choice for τ_{bin} is seen to correspond to where the contour lines in Fig. S5a start to become vertical. It seems reasonable that longer bins are sub-optimal because Fig. S5 suggests that no benefit from increased pump power is possible.

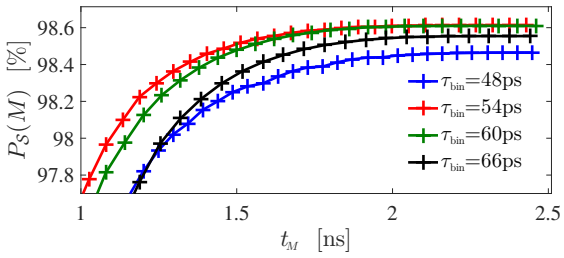

FIG. S8. Success probability as a function of t_M for different bin duration. The + markers indicate time-bin separations. Parameters are the same as in Fig. S6.

[S1] C. K. Madsen, G. Lenz, A. J. Bruce, M. A. Cappuzzo, L. T. Gomez, and R. E. Scotti, IEEE Photonics Technology Letters **11**, 1623 (1999).

[S2] C. J. McKinstrie, J. D. Harvey, S. Radic, and M. G. Raymer, Optics Express **13**, 9131 (2005).

[S3] Q. Li, M. Davanco, and K. Srinivasan, Nature Photonics **10**, 406 (2016), arXiv:1510.02527.

[S4] Z. Vernon, M. Liscidini, and J. E. Sipe, Physical Review A - Atomic, Molecular, and Optical Physics **94**, 1 (2016), arXiv:1606.01582.

[S5] C. Joshi, A. Farsi, S. Clemmen, S. Ramelow, and A. Gaeta, in *CLEO Technical Digest* (2016) pp. 4–5.

[S6] Y.-P. Huang, V. Velev, and P. Kumar, Optics Letters **38**, 2119 (2013).

[S7] J. R. Johansson, P. D. Nation, and F. Nori, Computer Physics Communications **184**, 1234 (2013).

[S8] H. Haus and W. Huang, Proceedings of the IEEE **79**, 1505 (1991).